Journal of Biomedical Optics 8(2), 281–287 (April 2003)

Optoacoustic imaging for optimization of laser cyclophotocoagulation

Uwe Oberheide
Ingo Bruder
Herbert Welling
Laser Zentrum Hannover e.V.
Hollerithallee 8
30419 Hannover, Germany
E-mail: uo@lzh.de

Wolfgang Ertmer
University of Hannover
Welfengarten 1
30167 Hannover, Germany

Holger Lubatschowski
Laser Zentrum Hannover e.V.
Hollerithallee 8
30419 Hannover, Germany

Abstract. Optoacoustic imaging was used for ophthalmic imaging, especially of the ciliary body region, which is of interest in the treatment of glaucoma. The different tissue structures below the sclera of porcine and rabbit eyes in vitro could be differentiated up to a depth of more than 1.5 mm. Based on the optoacoustic signals, two-dimensional tomographic images could be generated for visualization of this region in a B-scan mode. In addition, changes during the coagulation process could be measured in real time, allowing the development of online control mechanisms for cyclophotocoagulation, which is an important therapy of glaucoma. [DOI: 10.1117/1.1559998]

Keywords: medical imaging; ophthalmology; photoacoustics; piezoelectricity; transducers.

Paper 02010 received Feb. 22, 2002; revised manuscript received Sep. 20, 2002; accepted for publication Nov. 15, 2002.

1 Introduction

One of the main goals in medical diagnostics is the noninvasive imaging of biological tissues *in vivo* for the detection of diseased or altered tissue. Several methods, such as optical coherence tomography,[1] optical tomography,[2,3] or ultrasound echography[4] exist, each having its own particular advantages.

Furthermore, in many therapeutical applications of lasers, such as ablation or coagulation, the laser-tissue interaction occurs on a short timescale of only a few nano- to milliseconds. Therefore, it is extremely difficult to monitor changes in the optical properties of tissue in real time, to be able to use them, e.g., for control mechanism of the laser.

For nearly a decade, laser-induced ultrasound, or so-called optoacoustics, has been a subject of investigation to fulfill these tasks of imaging and control mechanism.[5–10] This method combines the advantages of ultrasound imaging and optical tomography. It uses the high absorption contrast of biological tissue, such as blood vessels and the surrounding skin. These absorbing structures act as ultrasound sources inside the tissue.

The generation of ultrasound allows for a deeper imaging penetration, since ultrasound waves are, in contrast to light, scattered and attenuated only weakly in tissue.

The principle of optoacoustics is depicted in Fig. 1. The tissue is irradiated with a pulsed light source with a typical pulse duration of a few nanoseconds. According to the optical properties of the tissue, a light distribution occurs, leading to thermoelastic expansion of the structures showing a higher absorption. This thermoelastic expansion generates a stress transient that propagates through the tissue at the speed of sound, and which can be detected at the surface of the tissue using either optical or piezoelectrical detectors. Using the time-dependant stress profile, conclusions concerning the absorbing structures can be drawn. The arrival time gives the depth of the structure via the speed of sound, whereas the amplitude and decay of the signal gives the optical properties (e.g., absorption and effective attenuation coefficient).

Ultrasonic detectors based on piezoelectric[11] or optical effects, such as the change of the refractive index,[12] can be used for detection of these phenomena.

In general, detection can be performed in two ways, either in forward mode with an irradiation source and detector on different sides of the tissue, or in backward mode with source and detector on the same side of the tissue (which is shown in Fig. 1). Due to accessibility, the backward mode is preferable for most tissues.

Our investigations focus on the feasibility of using optoacoustics for ophthalmic use, mainly for the treatment of glaucoma. For treatment of this ophthalmic disease, laser cyclophotocoagulation has become an established method during the last few decades.[13] The aim of this method is to coagulate the ciliary body, which is responsible for the production of aqueous humor of the eye, and thereby rebalance the production and drainage of the humor. The principle of this therapy is shown in Fig. 2. A pulsed Nd:YAG or diode laser serves as light source for the irradiation of the ciliary body. Radiation from such a laser is applied onto the sclera via an optical fiber with a tip diameter of typically 600 μm.

Typical therapeutic parameters are a few watts for one or two seconds.[14] The fiber is placed approximately 1.5 mm from the corneoscleral limbus, which is the interface between the transparent cornea and the white sclera. The main problems with this method arise from uncertainties in localizing the cilary body and in determination of the proper energy to be used. Furthermore, the short therapy duration of the therapy makes online monitoring of the coagulation process desirable, to avoid an overdosage or the necessity of retreatments. Existing methods for online monitoring of cyclophotocoagulation lack the possibility to localize the ciliary body.[14] In this work, experimental results of optoacoustic measurements considering both of these problems, localization as well as the online monitoring, are presented.

1083-3668/2003/$15.00 © 2003 SPIE

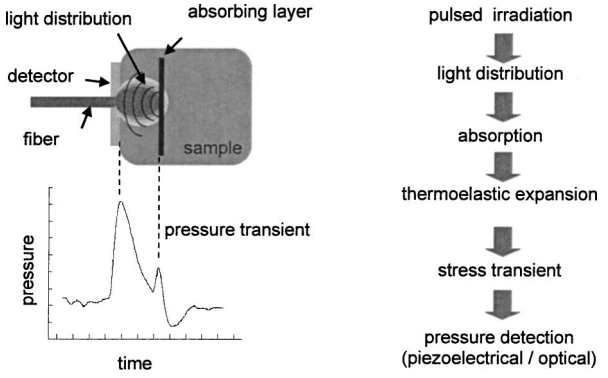

Fig. 1 Principle of laser optoacoustics in backward mode (irradiation and detection on the same side of the tissue) and the resulting signal.

2 Theoretical Description

For the process of laser-induced ultrasound generation, various theoretical descriptions have been published.[15,16] Therefore, only a brief description for mainly absorbing samples is given. The absorbed energy per volume $E_{abs}=\mu_a\Phi_0$ with the absorption coefficient of the tissue μ_a and the fluence Φ_0 is converted into an initial pressure distribution p via the Grueneisen coefficient $\Gamma=(\beta c_0^2)/C_p$, with the volumetric expansion coefficient β, the speed of sound c_0, and the heat capacity at constant pressure C_p [16]:

$$p=\Gamma E_{abs}. \tag{1}$$

For instantaneous pressure generation, the so-called stress confinement has to be fulfilled, which means that the laser pulse duration τ_L has to be short compared to the time the stress transient needs to propagate through the optical penetration depth at the speed of sound c_0:

$$\tau_L\cdot\mu_a\cdot c_0\ll 1. \tag{2}$$

In this case, no energy dissipation will occur during generation of the optoacoustic stress transient. The influence of longer pulse durations is described in detail in Ref. 15. The propagation of the stress transient through the tissue can be described using the Poisson formalism:[17,18]

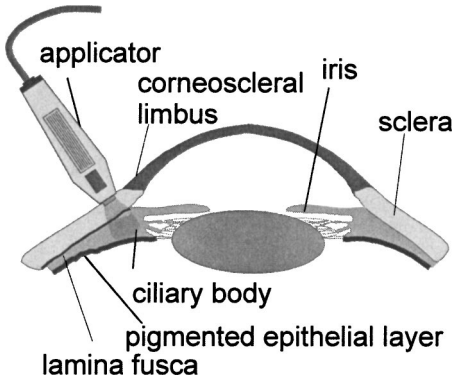

Fig. 2 Principle of laser cyclophotocoagulation. The ciliary body is coagulated using near-infrared light from a cw Nd:YAG or diode laser.

$$p(\vec{r},t)=\frac{1}{4\pi}\frac{\partial}{\partial t}t\int_0^{2\pi}d\Omega p_0(\vec{r},t)+\frac{1}{4\pi}t\int_0^{2\pi}d\Omega\frac{dp_0(\vec{r},t)}{dt}. \tag{3}$$

It describes propagation of the initial pressure distribution p_0 through the sample on spheres with the radius $r=c_0t$. A change of the detected pressure at a point r can only be measured after a time t if the surface of such a sphere touches or cuts the initial pressure distribution p_0. Therefore, Eq. (3) gives the spatial pressure distribution at any time t. To calculate this, the knowledge of two initial conditions is necessary. The first is the initial pressure distribution for $t=0$, and the second is the time derivative dp/dt of this initial distribution. Since this derivative is zero for an instantaneous pressure generation, the second term in Eq. (3) vanishes.

In this study, numerical simulations were performed using this formula on a layered tissue model consisting of three layers with the optical properties of rabbit sclera, ciliary body, and pigmented epithelium taken from the literature.[19] Table 1 gives an overview of the optical properties as well as the layer thicknesses. To determine the initial light distribution, a Monte Carlo simulation[20] was performed, yielding the absorbed-energy distribution used in Eq. (1).

With conversion into an initial pressure distribution p_0, the Poisson formula [Eq. (3)] for any detector geometry can be calculated. For the numerical calculation of Eq. (3), the following assumptions and simplifications were used.

- The rotational symmetry of the absorbed energy distribution allows use of an initial pressure distribution of the kind $p_0(\vec{R}+c_0t\vec{e}_r)$, with $\vec{R}$ being the vector to the detector spot and $\vec{e}_r$ the unity vector in spherical coordinates.
- The position of an ideal point detector is at the surface of the sample with the distance R from the irradiation axis leading to a modification of Eq. (3):

$$p(\vec{r},t)=\frac{1}{4\pi}\frac{\partial}{\partial t}t\int_0^{2\pi}d\Omega p_0(\vec{R}+c_0t\vec{e}_r)+\frac{1}{4\pi}t\int_0^{2\pi}d\Omega\frac{dp_0(\vec{R}+c_0t\vec{e}_r)}{dt}. \tag{4}$$

  The assumption of a point detector allows use of an ideal signal without diffraction and broadening of the signal.

- For calculations showing the qualitative influence of the parameters, the assumption of an instantaneous pressure generation corresponding to the stress confinement leads to $dp_0/dt=0$ (at $t=0$).

Due to the symmetry around the z axis, a two-dimensional replacement in spherical coordinates can be used with

$$\begin{bmatrix} x+c_0t\sin(\Theta)\cos(\varphi)\\ y+c_0t\sin(\Theta)\sin(\varphi)\\ z+c_0t\cos(\varphi)\end{bmatrix}\rightarrow\begin{bmatrix} R^2+c_0^2t^2\sin^2(\Theta)+2Rc_0t\sin(\Theta)\cos(\varphi)^{1/2}\\ z+c_0t\cos(\varphi)\end{bmatrix}=\begin{pmatrix} u\\ w\end{pmatrix}, \tag{5}$$

Table 1 Optical properties of rabbit eyes for a wavelength of 1064 nm,[19] used for the numerical calculations.

Tissue	μ_a (cm^{-1})	μ_s (cm^{-1})	g	thickness (μm)
Sclera	1.80	164.0	0.9	550
Ciliary muscle	4.75	516.1	0.9	290
Ciliary pigmented epithelium	94.00	0.0	0.9	10

yielding

$$p(\vec{R},t)=\frac{1}{4\pi}\int_0^{2\pi}d\varphi\int_{\pi/2}^{\pi}d\Theta\,\sin(\Theta)\left[p_0+t\frac{\partial p_0(u,w)}{\partial u}\frac{\partial u}{\partial t}+t\frac{\partial p_0(u,w)}{\partial w}\frac{\partial w}{\partial t}\right], \quad (6)$$

which can be solved numerically. Here, the lower boundary of the inner integral was set to $\pi/2$, assuming zero pressure above the surface of the sample.

Figure 3 shows the calculated absorbed-energy distribution for the ciliary body region of a rabbit eye, using the properties from Table 1. The beam has a diameter of 600 μm and a pulse energy of 10 mJ. Higher absorbed-energy densities are shown in bright colors, whereas the dark areas at the right side indicate only low absorbed-energy densities. The three different layers can be clearly distinguished, due to the stepwise increase of the absorbed-energy densities. Figure 4 shows the cross sections at two distances from the irradiation axis of Fig. 3 (top), and the calculated time-dependent pressure profiles (bottom) on top of the tissue sample at these distances.

It can be clearly seen that for larger distances from the axis, the separated pressure peaks from the ciliary body and the pigmented epithelium become one broadened peak, only showing a rough estimation of the depth of the ciliary body. Based on these calculations, it is obvious that for the localization of the ciliary body, the lateral distance between the irradiating fiber and detector should be short for optimal z resolution.

For online monitoring of the coagulation process, the influence of the temperature rise is very important. Under these circumstances, the volumetric expansion coefficient β cannot be considered to be constant, thus leading to a change in the Grueneisen-coefficient Γ, and therefore the conversion from absorbed energy into pressure.

A linear approximation of Γ was given by Landau and Lifschitz[17]

$$\Gamma=\frac{c^2}{C_p}\left[\beta(T_0)+\left(\frac{d\beta}{dT}\right)_{T_0}T'\right], \quad (7)$$

and agreed with experimental data.[21,22]

For a temperature gradient at the start of the coagulation process, the second term leads to an increasing Γ, and therefore higher optoacoustic signal amplitudes. Measurements on

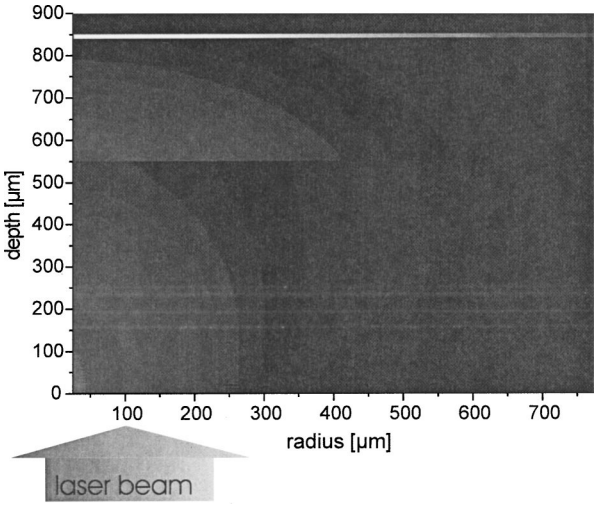

Fig. 3 Absorbed energy distribution derived from a Monte Carlo simulation for the ciliary body region of a rabbit eye. Bright colors indicate a higher absorbed energy density, and dark colors indicate a lower one. The arrows mark the irradiated area.

biological tissues showed a linear rise of the amplitude[22] in the range from 20 to 47 °C, although the optical attenuation coefficient stayed constant.

Due to the changes of the optical properties above a tissue temperature of approximately 55 °C, the influence of this process on the detected signal cannot be predicted completely. The whitening of most tissues during coagulation allows the assumption that the scattering coefficient increases

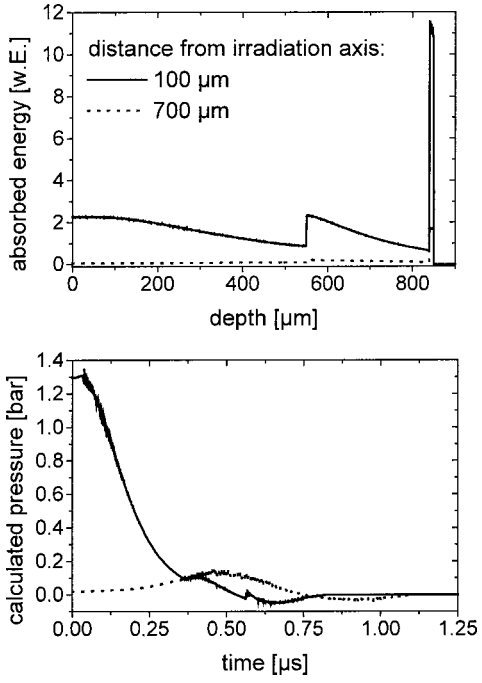

Fig. 4 Cross sections of Fig. 3 at two distances from the irradiation axis (top), and related, calculated time-dependent pressure profiles. Due to the larger distance, the signal detected 700 μm from the irradiation axis is broadened.

strongly.[23,24] This would affect the optoacoustic signals in a way that the amplitude should be decreased, and the entire signal will be broadened.

3 Materials and Methods

The experimental setup consists of a Q-switched Nd:YAG laser emitting at 1064 nm as source for the pulsed irradiation. The pulse duration is 33 ns. The emitted light is coupled into a silica fiber with a core diameter of 600 μm, which leads to the detector handpiece. The acoustic detector is made of a piezoelectric polyvinylidenfluoride (PVDF) film with a thickness of 9 μm. The film is covered on both sides with an aluminum coating used as electrodes to measure the charge separation of the piezoelectric film. The overlap of the two electrodes forms the active detector region, which is the pressure sensitive part of this detector. In these experiments the active area was a ring with an outer diameter of 900 μm and an inner diameter of 650 μm. The irradiating fiber is located in this inner part. To avoid signal distortions due to acoustic reflections at the back of the detector, the piezoelectric film is glued to a nonpolarized block of PVDF (Fig. 5). The typical bandwidth of the detector was 80 MHz, and the typical sensitivity was 6.6 mV/bar

The pressure transients are recorded with a fast oscilloscope (Tektronix TDS-540D) using an input impedance of 1 MΩ, or a transient recorder PC card (Fast Comtech TR 400) and a LabView program after amplification with a transimpedance converter and a voltage amplifier (Femto DHPVA-200) with an input impedance of 50 Ω.

Figure 5 shows the complete setup with an enlarged sketch of the detector head. Note that due to reasons of visibility, the depiction is not to scale.

A diode laser (SDL FD4200-25) emitting at a wavelength of 810 nm can be coupled into the same fiber to coagulate the tissue. Thus, tissue changes during laser treatment could be monitored online.

The tissue samples used for the experiments were either freshly enucleated porcine or rabbit eyeballs, which were used within five hours, to avoid changes due to degradation of the tissue. During measurement, a constant intraocular pressure of 21 mmHg was maintained by infusion of a physiological NaCl solution. The samples were fixed in a translation stage made of two plates with holes for the eyeglobe, to allow recording of optoacoustic transients at defined distances from the corneoscleral limbus. For the comparison of the imaged region with the real eyeglobe, histological sections from these parts were taken using an HE staining. Black surgical twine was sewed into the sclera at the starting and end point to mark the measured line for the histological section. This twine can be seen clearly in the histological sections, but is not shown in Fig. 6.

4 Experimental Results

4.1 *Localization of the Ciliary Body*

To localize the ciliary body of a porcine eye, 16 spots at a distance of 500 μm to each other arranged on a straight line perpendicular to the limbus were measured. The pulse energy of the Nd:YAG laser was 10 mJ at each measured spot. The transients measured were directly converted into a gray-scale

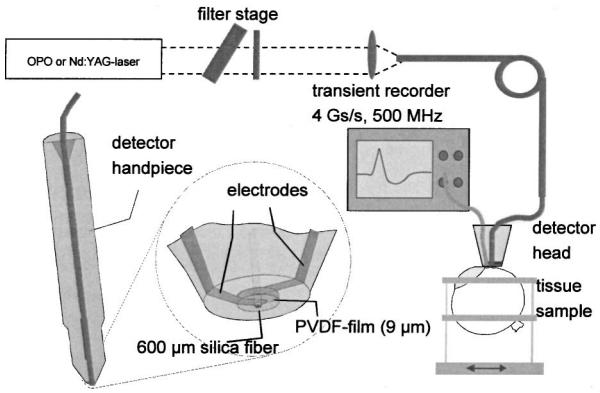

Fig. 5 Experimental setup used for the detection of optoacoustic transients on enucleated porcine and rabbit eyes. The magnification on the right side (not to scale) shows the detector head with a ring-shaped active area surrounding the fiber tip.

image with a linear color scale. Bright colors indicate regions with a high induced pressure amplitude, and therefore higher fluence and absorption coefficient, whereas dark colors indicate regions with low pressure amplitudes. Figure 6 shows the gray-scale image together with the corresponding histological section.

For comparison, the curved histological section was digitally corrected into a rectangular shape. A typical shrinkage of 4% was assumed, which means that the region between the two black twines was split into segments of 480 μm length, which were then realigned.

In the optoacoustic image, the course of the pigmented epithelium can be seen as a brighter line in the pars plana region (1) on the left side of the image, which splits into two pigmented layers at the ciliary body. These two layers, which have a high absorption at 1064 nm, are the ciliary pigmented epithelium (2) in the back, and the lamina fusca (3) in the front. The ciliary body (4) with lower absorption can be localized as a dark spot surrounded by these two layers. Due to the high scattering coefficient of the sclera, the fluence in this part is increased, leading to higher absorption and therefore a higher signal (5). Since the transparency increases from the pars plana region (on the left) towards the cornea (6) (on the right), the sclera signal decreases. However, this higher transparency allows for higher fluences in the underlying layer, i.e., the iris. Therefore, the generated optoacoustic signals from the iris (7) show high amplitudes.

Figure 7 shows optoacoustic transients extracted from the gray-scale image at three different locations, which are the detector positions 1, 9, and 12, respectively. In the signal from position 1, which is the pars plana region, peaks from the sclera after 0.2 μs, and from the pigmented epithelium after 0.55 μs, can be seen. At detector position 9, the signal from the pigmented epithelial layer broadens, due to the fact that it splits into lamina fusca and ciliary pigmented epithelium. These two layers can be clearly distinguished in the signal taken at detector position 12, which is located at the ciliary body region.

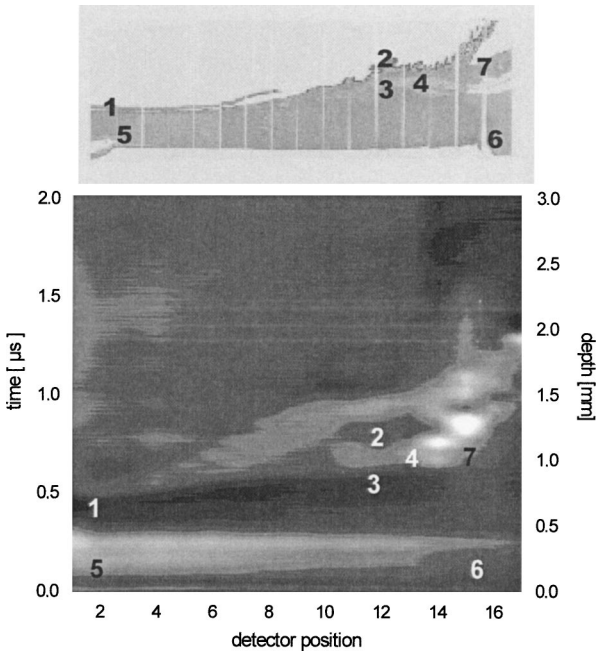

Fig. 6 Histological section of a rabbit eye and related tomographic image generated by optoacoustic transients at 16 positions with a spot separation of 500 μm. The course of the pigmented epithelial layer (1 to 3) can be clearly seen, indicating the position of the ciliary body.

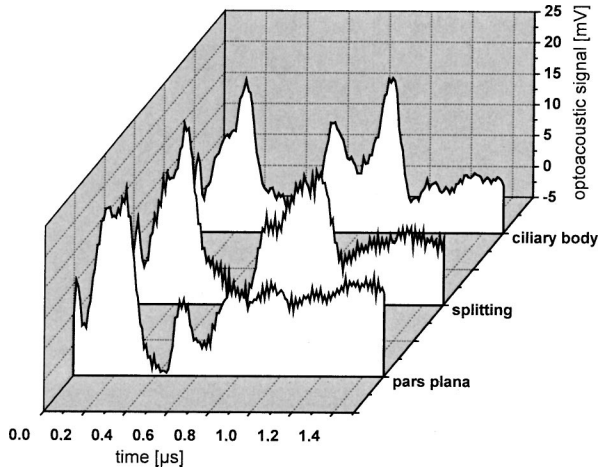

Fig. 7 Three optoacoustic transients from Fig. 6. The transients at the detector positions (from front to back) 1, 9, and 12 show splitting of the pigmented epithelial layer into two layers at the ciliary body.

4.2 *Tissue Alterations by Coagulation*

In addition to the tomographic measurements, laser optoacoustics are suitable for measuring changes in temperature,[25,26] and therefore changes of the tissue due to coagulation.

To apply this to the therapy of laser cyclophotocoagulation, gray-scale images, such as in Fig. 6, of a porcine eye were measured before and after coagulation of the ciliary body region. The ciliary body region was localized as described before, and the tip of a pig-tailed laser diode was placed 1.5 mm from the corneoscleral limbus. A laser power of 1 W was applied for 5 s to generate a coagulated tissue area in the ciliary body as well as the ciliary pigmented epithelium (CPE).

Figure 8 shows the corresponding gray-scale images of the porcine eye. To generate the optoacoustic transients, a pulse energy of 10 mJ was applied. In the image used for localization (top), the CPE and the lamina fusca can be seen again as thin gray bands (1 resp. 2). In the gray-scaled image of the ciliary body after coagulation, a darker area, which indicates a lower absorption, can be observed where the irradiation was

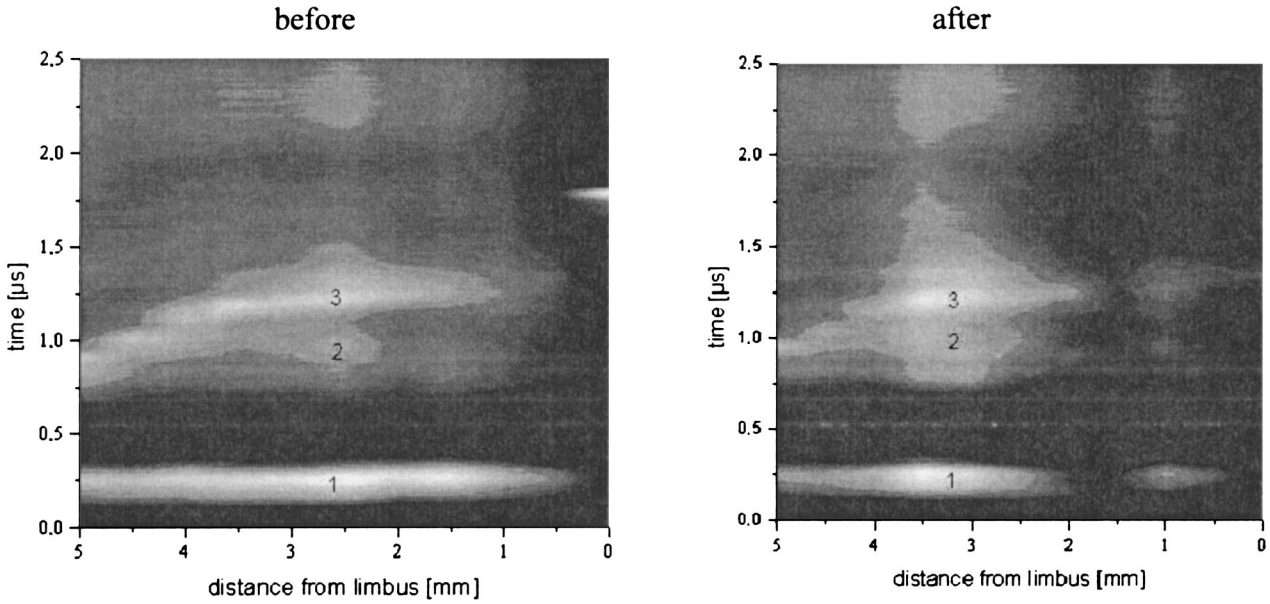

Fig. 8 Optoacoustic tomographic images of the ciliary body region of a porcine eye before and after coagulation. The fiber tip for coagulation was placed 1.5 mm from the corneoscleral limbus. The changes in the gray-scale image due to coagulation can be clearly seen as darker areas corresponding to a decreased optoacoustic signal.

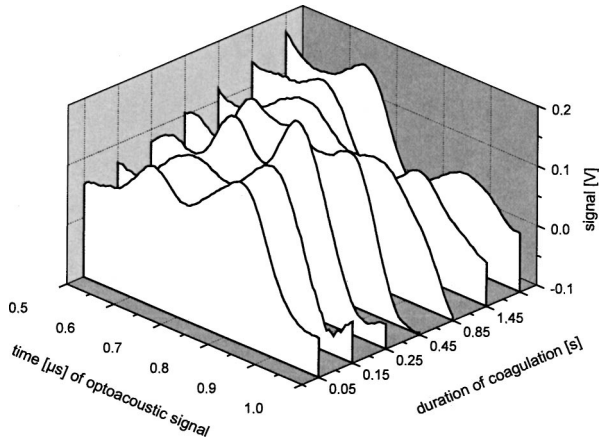

Fig. 9 Optoacoustic transients of the ciliary body region of a rabbit eye measured in real time during the coagulation process. The increase in amplitude due to the temperature rise can be seen, as well as the following decay due to the changes of the optical properties.

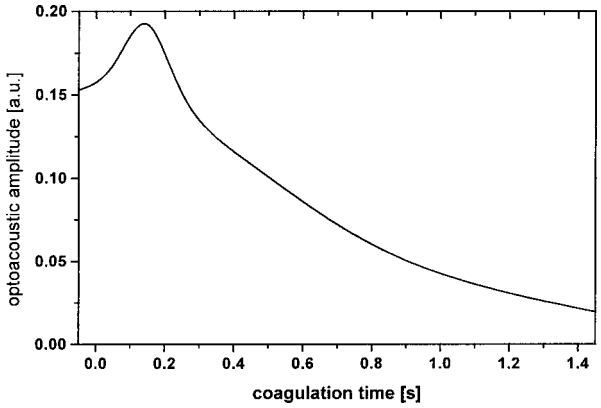

Fig. 10 Time dependence of the optoacoustic amplitude (from Fig. 9) during the coagulation process.

applied. This corresponds to the predictions that coagulation should increase the scattering coefficient,[23,24] leading to lower fluence at the CPE, and therefore lower pressure transients, although for coagulated skin a decreased scattering was reported.[27]

The time dependence of these changes of the ciliary body of a rabbit eye are shown in Fig. 9. Optoacoustic transients from the ciliary body region were recorded every 100 ms, corresponding to the repetition rate of 10 Hz of the Nd:YAG laser, before and during the coagulation process. A power of 2 W from the diode laser was applied with the same fiber as the pulses used for the generation of the optoacoustic signals. The duration of the coagulation was 2 s. To generate the optoacoustic signals, a pulse energy of 7 mJ was used. Figure 9 shows, from front to back, transients before the coagulation process and after 0.05, 0.15, 0.25, 0.45, 0.85, and 1.45 s duration of coagulation. In Fig. 10, the amplitude of the optoacoustic signal for each transient from the CPE, e.g., the peak at approximately 0.8 μs of each transient, is plotted versus the coagulation time. The course follows the predictions that for short terms the amplitude increases, due to the temperature rise and the increasing Grueneisen coefficient. For longer time periods, the maximal amplitude decreases strongly due to the changes in absorption and especially scattering coefficients of the tissue. The measurements finally lead to the same result as shown in Fig. 8.

5 Conclusions

From the actual results, laser optoacoustics seem to be a promising tool for localization of the ciliary body. Image processing of the measured signals allows a tomographic view of the internal structures below the sclera with a depth of more than 1.5 mm. Although the axial resolution of the piezoelectric detector used is limited to more than 50 μm, due to the high scattering in the tissue and the limited bandwidth of the detector, the pigmented epithelium with a thickness of 10 μm can be localized. The located structures correspond well with the histological sections.

For an enhanced and faster imaging procedure, the immediate detection of a complete line is necessary. Such a detector device consisting of eight detectors in a row has previously been constructed. First measurements with this system on tissue phantoms[28] show the potential of such arrays for biomedical imaging.

Furthermore, changes in the optical parameters of the tissue due to coagulation can be detected in real time, for example in the therapy of laser cyclophotocoagulation. Due to the increased temperature, the optocacoustic signal amplitude increases for small temperature rises up to approx. 45 °C. However, for longer coagulation periods, the changes in the optical properties do not allow a prediction of the acoustic transients yet. From the results, a qualitative control mechanism can be developed to prevent an overdosage of the laser power for treatment of glaucoma. Other concerns of clinical implementation such as eye movement and tissue perfusion can be neglected, due to the short application time of a few seconds. The energies of 10 mJ per pulse are far below the threshold level of tissue changes, and even pulse energies of up to 19 mJ do not show any influence on optical or mechanical parameters of the tissue.

Acknowledgments

The work has been supported by the Federal Ministry of Education and Research, Germany (BMBF) under grant 13N7242.

References

1. S. A. Boppart, B. E. Bouma, C. Pitris, J. F. Southern, M. E. Brezinski, and J. G. Fujimoto, ''In vivo cellular optical coherence tomography imaging,'' *Nat. Med.* **4**, 861–865 (1998).
2. B. Chance, K. Kang, L. He, J. Liu, and S. Zhou, ''Precision localization of hidden absorbers in body tissues with phased-array optical systems,'' *Rev. Sci. Instrum.* **67**, 4324–4332 (1996).
3. A. Yodh and B. Chance, ''Spectroscopy and imaging with diffusing photons,'' *Phys. Today* **48**, 34–40 (1995).
4. H. A. McCann, J. C. Sharp, T. M. Kinter, C. N. McEwan, C. Barillot, and J. F. Greenleaf, ''Multidimensional ultrasonic imaging for cardiology,'' *Proc. IEEE* **76**, 1063–1072 (1988).
5. A. Oraevsky, S. L. Jacques, and F. Tittel, ''Determination of tissue optical properties by piezoelectric detection of laser-induced stress waves,'' *Proc. SPIE* **1882**, 86–96 (1993).
6. A. Karabutov, V. Letokhov, and N. Podymova, ''Time-resolved optoacoustic tomography of inhomogeneous media,'' *Proc. SPIE* **2389**, 209–217 (1995).
7. R. Esenaliev, A. Oraevsky, S. Jacques, and F. Tittel, ''Laser opto-

acoustic tomography for medical diagnostics: experiments with biological tissues,'' *Proc. SPIE* **2676**, 84–90 (1996).
8. G. Paltauf and H. Schmidt-Kloiber, ''Photoacoustic determination of tissue optical properties and structure by use of an optical parametric oscillator,'' *Proc. SPIE* **3195**, 70–78 (1998).
9. K. Köstli, M. Frenz, H. Weber, G. Paltauf, and H. Schmidt-Kloiber, ''Optoacoustic infrared spectroscopy of soft tissue,'' *J. Appl. Phys.* **88**(3), 1632–1637 (2000).
10. U. Oberheide, B. Jansen, I. Bruder, H. Lubatschowski, H. Welling, and W. Ertmer, ''Optoacoustic online control for laser cyclophotocoagulation,'' *Proc. SPIE* **4256**, 53–60 (2001).
11. A. A. Oraevsky and A. Karabutov, ''Ultimate sensitivity of time-resolved opto-acoustic detection,'' *Proc. SPIE* **3916**, 228–239 (2000).
12. G. Paltauf, H. Schmidt-Kloiber, K. P. Koestli, and M. Frenz, ''Two-dimensional recording of optoacoustic waves,'' *Proc. SPIE* **3601**, 248–255 (1999).
13. J. M. Mastrobattista and M. Luntz, ''Ciliary body ablation: where are we and how did we get here?'' *Surv. Ophthalmol.* **41**(3), 193–213 (1996).
14. R. P. Preußner, ''Kontrollierte Zyklophotokoagulation,'' *Ophthalmologe* **95**, 645–650 (1998).
15. A. A. Karabutov, N. B. Podymova, and V. S. Letokhov, ''Time-resolved laser optoacoustic tomography of inhomogeneous media,'' *Appl. Phys. B: Lasers Opt.* **63**, 545–563 (1996).
16. V. Gusev and A. Karabutov, *Laser Optoacoustics*, AIP Press, New York (1992).
17. L. D. Landau and E. M. Lifschitz, Lehrbuch der theoretischen Physik Bd. 6, Akademie-Verlag Berlin (1978).
18. G. Paltauf and H. Schmidt-Kloiber, ''Photoacoustic cavitation in sperical and cylindrical absorbers,'' *Appl. Phys. A: Mater. Sci. Process.* **68**, 525–531 (1999).
19. B. Nemati, A. Dunn, A. J. Welch, and H. G. Rylander, ''Optical model for light distribution during transscleral cyclophotocoagulation,'' *Appl. Opt.* **37**(4), 764–771 (1998).
20. L. Wang and S. L. Jacques, ''Monte carlo modeling of light transport in multi-layered tissues in standard c,'' Technical Report, University of Texas M.D. Anderson Cancer Center (1995). http://ee.ogi.edu/omlc/science/mc/index.html.
21. G. Paltauf and H. Schmidt-Kloiber, ''Microcavity dynamics during laser-induced spallation of liquids and gels,'' *Appl. Phys. A: Solids Surf.* **62**, 303–311 (1990).
22. K. Larin, I. Larina, M. Motamedi, and R. O. Esenaliev, ''Monitoring of temperature distribution in tissues with optoacoustic technique in real time,'' *Proc. SPIE* **3916**, 311–321 (2000).
23. S. Jaywant, B. Wilson, M. Patterson, and L. Lilge, ''Temperature dependent changes in the optical absorption and scattering spectra of tissues: correlation with ultrastructure,'' *Proc. SPIE* **1882**, 218–229 (1993).
24. A. Roggan, H. Albrecht, K. Dörschel, and O. Minet, ''Experimental set-up and Monte-Carlo model for the determination of optical tissue properties in the wavelength range 330-1100 nm,'' *Proc. SPIE* **2323**, 21–36 (1995).
25. R. O. Esenaliev, I. Larina, K. Larin, and M. Motamedi, ''Real-time optoacoustic monitoring during thermotherapy,'' *Proc. SPIE* **3916**, 302–310 (2000).
26. G. Schüle, G. Hüttmann, J. Roider, and C. Wirbelauer, ''Optoacoustic measurements during μs-irradiation of the retinal pigment epithelium,'' *Proc. SPIE* **3914**, 230–236 (2000).
27. S. L. Thomson, H. Vijverberg, S. L. Jacques, and A. A. Oraevsky, ''Optical properties of albino rat skin in vitro: Comparison of photoacoustic and integrating sphere measurement techniques,'' *Proc. SPIE* **2134**, 106–113 (1994).
28. U. Oberheide, C. Lee, R. Krebs, H. Welling, W. Ertmer, and H. Lubatschowski, ''Two-dimensional detection of optoacoustic stress transients,'' *Proc. SPIE* **4618**, 99–105 (2002).